Journal of Magnetic Resonance 213 (2011) 158–165

Contents lists available at SciVerse ScienceDirect

Journal of Magnetic Resonance

journal homepage: www.elsevier.com/locate/jmr

High-frequency and -field EPR and FDMRS study of the $[Fe(H_2O)_6]^{2+}$ ion in ferrous fluorosilicate

J. Krzystek [a], D. Smirnov [a], Christoph Schlegel [b], Joris van Slageren [b,1], Joshua Telser [c], Andrew Ozarowski [a,*]

[a] National High Magnetic Field Laboratory, Florida State University, Tallahassee, FL 32310, USA
[b] 1. Physikalisches Institut, Universität Stuttgart, Pfaffenwaldring 57, D-70550 Stuttgart, Germany
[c] Department of Biological, Chemical and Physical Sciences, Roosevelt University, Chicago, IL 60605, USA

ARTICLE INFO

Article history:
Received 4 July 2011
Revised 24 August 2011
Available online 29 September 2011

Keywords:
High-field EPR
Spin Hamiltonian
Zero-field splitting
Iron(II)

ABSTRACT

The complex $[Fe(H_2O)_6]SiF_6$ is one of the most stable and best characterized high-spin Fe(II) salts and as such, is a paradigm for the study of this important transition metal ion. We describe high-frequency and -field electron paramagnetic resonance studies of both pure $[Fe(H_2O)_6]SiF_6$ and $[Zn(H_2O)_6]SiF_6$ doped with 8% of Fe(II). In addition, frequency domain magnetic resonance spectroscopy was applied to these samples. High signal-to-noise, high resolution spectra were recorded which allowed an accurate determination of spin Hamiltonian parameters for Fe(II) in each of these two, related, environments. For pure $[Fe(H_2O)_6]SiF_6$, the following parameters were obtained: $D = +11.95(1)\ cm^{-1}$, $E = 0.658(4)\ cm^{-1}$, $g = [2.099(4), 2.151(5), 1.997(3)]$, along with fourth-order zero-field splitting parameters: $B_4^0 = 17(1) \times 10^{-4}\ cm^{-1}$ and $B_4^4 = 18(4) \times 10^{-4}\ cm^{-1}$, which are rarely obtainable by any technique. For the doped complex, $D = +13.42(1)\ cm^{-1}$, $E = 0.05(1)\ cm^{-1}$, $g = [2.25(1), 2.22(1), 2.23(1)]$. These parameters are in good agreement with those obtained using other techniques. Ligand-field theory was used to analyze the electronic absorption data for $[Fe(H_2O)_6]SiF_6$ and suggests that the ground state is $^5A_1$, which allows successful use of a spin Hamiltonian model. Density functional theory and unrestricted Hartree–Fock calculations were performed which, in the case of latter, reproduced the spin Hamiltonian parameters very well for the doped complex.

1. Introduction

Iron is among the metal elements most important to all life on Earth. It is present in innumerable biochemical cycles, starting with the breathing cycle of mammals. During those cycles, it forms a variety of coordination complexes that are present primarily in two oxidation states: Fe(II) (ferrous, $3d^6$) and Fe(III) (ferric, $3d^5$). While the Kramers-type (half-integer spin number) ferric ion is generally amendable to Electron Paramagnetic Resonance (EPR) at conventional frequencies (9–95 GHz) and fields (0–3.5 T), the non-Kramers (integer spin) ferrous ion presents a considerable challenge to spectroscopists. When in the low-spin form ($S = 0$), it is diamagnetic and thus not amenable to EPR; however, even in the paramagnetic intermediate ($S = 1$) spin, or more commonly, high ($S = 2$) spin (HS) state it is difficult, or impossible to detect by EPR. This is because in reduced symmetry environments anisotropic orbital angular momentum contributions cause the phenomenon of zero-field splitting (zfs). Zfs removes the degeneracy of the $\langle S, M_S|$ levels, even in the absence of an applied magnetic field, and, in the case of HS Fe(II), can reach tens of cm^{-1}. It is often possible to employ EPR at conventional frequencies (X- or Q-band) to observe a nominally forbidden ($\Delta M_S = 4$, enhanced in parallel mode EPR) transition within the slightly split $|S, M_S\rangle = |2, \pm 2\rangle$ non-Kramers doublet, which usually occurs at very low applied magnetic field (below ¼ of the resonance field for $g = 2$). This "X-band active" transition has been productively investigated in certain HS Fe(II) systems [1–3]; however, it is of limited use in obtaining the complete set of spin Hamiltonian parameters.

To overcome the effect of zfs, either high frequencies or high magnetic fields are generally necessary for a successful detection of allowed ($\Delta M_S = \pm 1$) resonances. This was recognized early on by several researchers and resulted in a series of remarkable papers which were well ahead of their time [4–7]. Those impressive early works were not immediately continued, presumably because of persisting instrumental difficulties. It is only with recent technological progress, both in the development of easy-to-use, stable sub-THz wave sources and "user-friendly" sweepable superconducting and resistive magnets, that a series of papers on HS Fe(II) in various coordination environments has come out [8–11]. Most

* Corresponding author. Fax: +1 850 644 1366.
E-mail address: ozarowsk@magnet.fsu.edu (A. Ozarowski).
[1] Present address: Institut für Physikalische Chemie, Universität Stuttgart, Pfaffenwaldring 55, D-70569 Stuttgart, Germany.

1090-7807/$ - see front matter © 2011 Elsevier Inc. All rights reserved.
doi:10.1016/j.jmr.2011.09.046

notable of the recent work is that of Barra et al. on an actual metalloenzyme, reduced rubredoxin [12].

The recurrent motive of the early EPR papers on HS Fe(II) was the use of a ferrous salt, $[Fe(H_2O)_6]SiF_6$, in which Fe(II) exists in the form of hexaaquaferrous ion, as a standard [2,4,6,7,13]. This is a chemically relatively stable (resistant towards oxidation) form of HS Fe(II), and apparently, this salt produces a particularly strong and well defined EPR response both in conventional X- and Q-band EPR, and at frequencies in the sub-THz and THz region. The fundamental interest in $[Fe(H_2O)_6]SiF_6$ as a model system has not been limited to EPR spectroscopists; its electronic structure and particularly the magnetic properties of its lowest electronic state were investigated by an impressive variety of experimental methods: magnetometry [14–18], magnetic circular dichroism (MCD) [19], electronic absorption spectroscopy [20], electronic Raman spectroscopy [21], Mössbauer spectroscopy [22,23], and nuclear magnetic resonance [23]. These experimental studies spurred in turn several theoretical works [24–26]. That the interest in the magnetic properties of the basic $[Fe(H_2O)_6]SiF_6$ system has not waned with time is witnessed by a very recent paper [27]. With several other HS Fe(II) complexes now characterized in the literature by high-frequency and -field EPR (HFEPR), we decided to return to ferrous fluorosilicate to check the accuracy of the spin Hamiltonian parameters reported in the literature, compare them to other known Fe(II) complexes, and relate the most recent HFEPR technology to that available to the researchers back in the 1970s and 1980s. Since the literature covers experiments on both pure $[Fe(H_2O)_6]SiF_6$ salt and one in which Fe(II) was doped into diamagnetic $[Zn(H_2O)_6]SiF_6$, we prepared and investigated samples of both pure (100%) salt, and a doped system with 8% Fe(II): $[Fe_{0.08}Zn_{0.92}(H_2O)_6]SiF_6$. We also have used computational methods not readily accessible in those times to further understand the electronic structure of the hexaaquaferrous ion.

2. Experimental

2.1. Samples and crystal structures

Metallic iron was dissolved in hot 25% hexafluorosilicic acid (both from Acros). The product which crystallized upon cooling the solution was filtered and dried under nitrogen to yield polycrystalline $[Fe(H_2O)_6]SiF_6$. A similar procedure was used to prepare $[Zn(H_2O)_6]SiF_6$. A hot solution containing both salts at a ratio 8:92 yielded upon quick cooling the doped product $[Fe_{0.08}Zn_{0.92}(H_2O)_6]SiF_6$. The crystal structure of $[Fe(H_2O)_6]SiF_6$ at room temperature has been determined using X-ray diffraction [28] and refined by neutron diffraction [29]. According to the latter, there are two randomly distributed lattices, related by mirror planes belonging to the space group $D^5_{3d}(R\bar{3}m)$ and the iron(II) ion is positioned in a trigonally distorted octahedron of water molecules. Later studies suggested that upon lowering the temperature, a phase transition to a new structure characterized by a lower symmetry occurs [23]. The low-temperature phase was identified by X-ray diffraction [30,31] as belonging to the space group $C^5_{2h}(P2_1/c)$, and the transition temperature estimated to occur at about 240–255 K – a temperature well above what can be employed for HFEPR in this system. However, the molecular structure of this low-temperature, low-symmetry phase of $[Fe(H_2O)_6]SiF_6$ has not been reported to our best knowledge. This information would be desirable, derived from low temperature both X-ray and neutron diffraction, but is outside the scope of the present study.

The structure of $[Zn(H_2O)_6]SiF_6$ was published by Ray et al. [32]. It is typical of the $[M^{II}(H_2O)_6]SiF_6$ series (space group $R\bar{3}$, No.148), and has not been observed to undergo a phase transition to a low-symmetry, low-temperature phase. Thus the structure of the doped material studied by HFEPR at low temperature is that crystallographically determined.

2.2. Apparatus

HFEPR spectra were obtained using two spectrometers described in detail in the literature: one based on a set of backward wave oscillators operating in a 150–700 GHz frequency range, and a resistive 25-T "Keck" magnet [33], and another based on a superconducting 17-T magnet, described in [34], and using a Virginia Diodes Inc. source operating at a base frequency of 12–14 GHz, increased by a cascade of multipliers. X-band EPR was performed on a commercial Bruker Elexsys 680X instrument equipped with a dual-mode resonator. Frequency-domain magnetic resonance spectroscopy (FDMRS) spectra were recorded at Stuttgart University on a plane parallel pressed powder sample of $[Fe_{0.08}Zn_{0.92}(H_2O)_6]SiF_6$ at frequencies $\nu = 250$–530 GHz at $T = 5$ K, using a continuous-wave (cw) THz spectrometer that has been described in the literature [35]. A similarly pressed powder sample of $[Fe(H_2O)_6]SiF_6$ was studied at $\nu = 200$–515 GHz at $T = 1.5$ K in a newly assembled zero-field FDMRS spectrometer at NHMFL, Tallahassee, FL, which is built upon the same principles as the Stuttgart instrument.

Diffuse reflectance UV–Visible–NIR spectra of $[M(H_2O)_6]SiF_6$, M = Fe, Zn, were recorded at room temperature on a Jasco V-570 spectrometer using MgO as a diluent at Roosevelt University.

2.3. Data analysis

To analyze the EPR spectra of $[Fe_{0.08}Zn_{0.92}(H_2O)_6]SiF_6$, we applied the usual spin Hamiltonian for an $S = 2$ spin state including the second-order zfs terms [36]:

$$\mathscr{H} = \beta B \cdot \mathbf{g} \cdot S + D(S_z^2 - S(S+1)/3) + E(S_x^2 - S_y^2) \quad (1)$$

where β is the Bohr magneton and the other symbols take their usual meanings. The data quality for pure $[Fe(H_2O)_6]SiF_6$ were high enough to add fourth-order terms into the spin Hamiltonian, which thus becomes:

$$\mathscr{H} = \beta B \cdot \mathbf{g} \cdot S + D(S_z^2 - S(S+1)/3) + E(S_x^2 - S_y^2) + B_4^0 O_4^0 + B_4^2 O_4^2 + B_4^4 O_4^4 \quad (2)$$

The spin Hamiltonian parameters were *simultaneously* fitted to a 2-dimensional map of resonances vs. transition frequency (or energy) as opposed to single-frequency spectra. More details on the tunable-frequency EPR method used in this work can be found elsewhere [11,37].

Locally written programs employing a ligand-field theory (LFT) model with the full d^6 basis set were used to analyze the optical transitions reported for $[Fe(H_2O)_6]SiF_6$.

2.4. Quantum chemistry calculations

The known crystal structures of $[Fe(H_2O)_6]SiF_6$ [29] and $[Zn(H_2O)_6]SiF_6$ [32] were used in the density functional theory (DFT) and unrestricted Hartree–Fock (UHF) calculations employing the freely available ORCA 2.8 software designed by Neese [38]. The calculations utilized the Ahlrichs type basis sets [39] VDZ and TZV [40] combined with the BP86 functional [41–45].

3. Results and discussion

3.1. HFEPR spectroscopy of $[Fe(H_2O)_6]SiF_6$

As expected, pure $[Fe(H_2O)_6]SiF_6$ produced a strong EPR response in the 150–700 GHz frequency range at low temperatures.

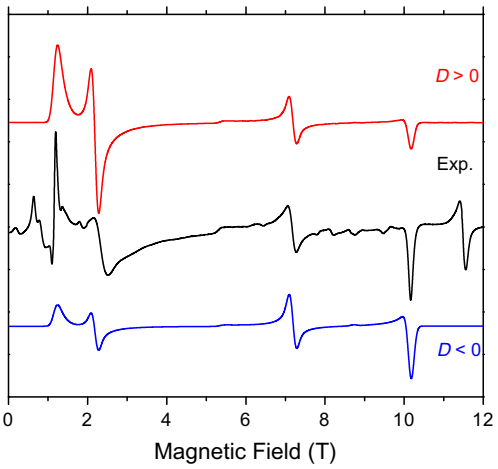

Fig. 1. An HFEPR spectrum of pure $[Fe(H_2O)_6]SiF_6$ powder at 321.6 GHz and 20 K (black trace) accompanied by simulations using the zfs parameters of Champion and Sievers [6] ($S = 2$, $|D| = 11.67$, $|E| = 0.67$ cm^{-1}) and adjusted g-values: $g_\perp = 2.15$; $g_{||} = 2.00$. Colored traces are simulations using a positive (red trace); or negative D (blue trace). Single-crystal linewidth: 75 mT (isotropic). The resonance at 11.5 T ($g = 2.00$) originates from impurities (Mn(II) and presumably Fe(III)) and is not simulated. (For interpretation of the references to color in this figure legend, the reader is referred to the web version of this article.)

Fig. 1 shows a representative spectrum of a powder sample at 321.6 GHz and 20 K, recorded in a superconducting magnet, together with simulations. The spin Hamiltonian parameters used in the simulations were those of Champion and Sievers [6], which reproduce the spectra very well when g-values of $g_\perp = 2.15$; $g_{||} = 2.00$ are assumed. Despite the obvious artifacts observed at low field due to an imperfectly random distribution of crystallites in the sample, the simulations agree better with experiment when a positive sign of D is assumed. This was more convincingly confirmed at other frequencies, and temperatures (see Fig. S1 in the Supplementary Information).

Because spin Hamiltonian parameters optimized for single-frequency simulations are often frequency-dependent, we have performed HFEPR at multiple frequencies, and combined the results into a single set of resonances, which we then used to fit the parameters [37]. The resulting 2-D map (field vs. frequency, Fig. 2) is characteristic for a quintet ($S = 2$) state with $D \sim 12$ cm^{-1}, and a small rhombic zfs parameter E. In particular, the two zero-field resonances indicated near 300 and 415 GHz correspond to the $|D - 3E|$ and $|D + 3E|$ transitions and by themselves could yield the second-order zfs parameters. However, a computer fit to the complete 2-D map yields parameters (Table 1) of superior quality, and it also delivers the g-matrix, which is not possible in zero field. Additionally, including the 4th order parameter B_4^0 of $17(2) \times 10^{-4}$ cm^{-1} improved the fit quality as seen by the 46% smaller fit error. The effect of this fourth order term is not readily seen in Fig. 2; to demonstrate this, we present in Supporting Information (Fig. S2) a comparison of experimental and calculated points both with and without the B_4^0 term. The sign of B_4^0 must be the same as that of D, namely positive.

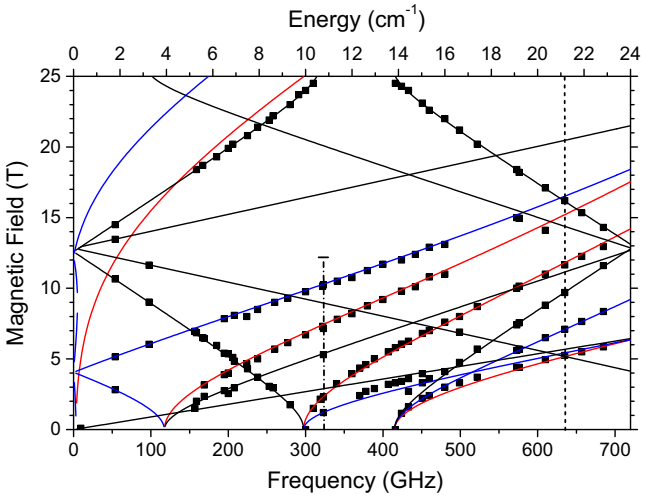

Fig. 2. Field/frequency map of resonances in pure $[Fe(H_2O)_6]SiF_6$ powder at 10 K. Squares are experimental points while the curves were calculated using the best-fitted spin Hamiltonian parameters as in Table 1. Red traces: resonances with $B_0 \,||\, x$, blue traces: with $B_0 \,||\, y$, black traces: $B_0 \,||\, z$. The lone square at 9.4 GHz is the "X-band active resonance" shown in Fig. 3. The vertical dashed line at 321.6 GHz represents the frequency and field range of the spectrum shown in Fig. 1, while that at 635 GHz represents the parameters of the spectrum shown in Fig. S1 in the Supplementary Information. The effect of the fourth order term, B_4^0, is shown in Fig. S2 in the Supplementary Material. (For interpretation of the references to color in this figure legend, the reader is referred to the web version of this article.)

Fig. 2 presents experimental data and calculated lines corresponding only to the canonical (x,y,z) orientations. Off-axis (non-canonical) turning points do contribute to the observed powder spectrum; however, the effective orientation of these turning points depends on frequency and thus it is very difficult to use them in fitting the spin Hamiltonian parameters using the 2-D maps. Therefore only those features in the powder spectra which can be assigned to the axial turning points have been taken into account in such fits in the present paper. We have in other cases seen off-axis transitions and occasionally used them in fits [46]. The Supporting Information presents simulations that show the relations between the powder spectrum patterns and the axial as well as off-axial turning points, for rotations about the x (Fig. S3) and y (Fig. S4) axes for a representative experimental spectrum (216 GHz, 50 K).

We also undertook to check how the zfs parameters obtained from a multi-frequency fit reproduce the "X-band active transition". The corresponding spectrum is shown in Fig. 3, using parallel-mode detection. It is accompanied by two simulations: one using the spin Hamiltonian parameters determined from HFEPR experiments and seen in Table 1 but ignoring the fourth-order zfs parameter B_4^4, the other including $B_4^4 = 18 \times 10^{-4}$ cm^{-1}. Despite the presence of impurities (specifically, HS Co(II) which is responsible for the partly resolved hyperfine structure near 0.1 T) and some possible artifacts due to an imperfect powder, the agreement between the experiment and simulations obtained with HFEPR parameters is very good but only when a finite value (positive, as with B_4^0) of the fourth-order zfs parameter B_4^4 of 18×10^{-4} cm^{-1} is taken into account, which makes the calculated peak maximum correspond exactly with experiment (see Fig. 3). Since $B_4^4 O_4^4$ mixes the nominal $M_S = \pm 2$ states, B_4^4 has the greatest effect on the position of the "X-band active transition" of all spin Hamiltonian parameters. Rubins and Black also found the need to include this fourth order zfs term [13], although fourth-order zfs terms were not taken into consideration by Hendrich and Debrunner [1,2]. The fourth order term, B_4^2, could also be present, but its inclusion changes the other parameters very slightly and only marginally improves (by 1%) the average deviation between the calculated and experimental points, while the estimated error in B_4^2 is comparable to its magnitude ($B_4^2 = -0.005(3)$ cm^{-1}).

This combination of the X-band data with multi-frequency high-field spectra allows one to determine an essentially unique set of spin Hamiltonian parameters, including fourth order terms. The reverse procedure, however, i.e., obtaining dependable values for the complete set of spin Hamiltonian parameters from the "X-band active transition" alone is not feasible as it is not possible to separate the contributions of second and fourth order zfs. Some of us have earlier demonstrated this difficulty

Table 1
Spin Hamiltonian parameters for pure $[Fe(H_2O)_6]SiF_6$. All zfs values are in cm^{-1}.

D	$\|E\|$	B_4^0	B_4^4	g_x	g_y	g_z	Technique
+11.95(1)	0.658(4)	$17(1)\times10^{-4}$	$18(4)\times10^{-4}$	2.099(4)	2.151(5)	1.997(3)	HFEPR, this work [a]
+11.93(2)	0.662(6)	0	$18(4)\times10^{-4}$	2.09(1)	2.15(1)	2.003(5)	
11.88	0.68						FDMRS, this work
11.78	0.67						FDMRS [b]
11.88	0.67					1.96	FDMRS, HFEPR [c]
12.3(2)	0.53						Magnetization [d]
10.9				2.12	2.12	2.00	Magnetization [e]
−10.4				2.14	2.14	2.00	Magnetization [f],
11.95	0.68						Raman [g]

[a] Two sets of fit parameters are presented. The first is with B_4^4 fixed at 18×10^{-4} (this value is based on fitting the X-band signal; its error is estimated visually; all other errors are based on statistical analysis of the fits (Hessian matrix)) with all other parameters variable; the second set is with B_4^0 fixed at zero, all other parameters variable. The average (rms) deviation of the calculated resonance fields from experimental values is 1.8 times higher in the second fit than in the first.
[b] Ref. [6].
[c] Ref. [7].
[d] Ref. [16].
[e] Ref. [14].
[f] Ref. [15].
[g] Ref. [21].

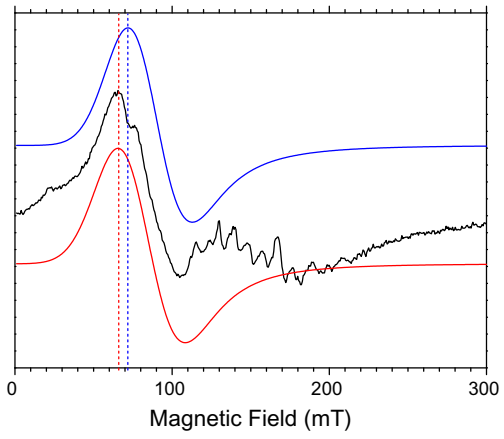

Fig. 3. Parallel-mode X-band EPR spectrum of $[Fe(H_2O)_6]SiF_6$ powder recorded at 9.415 GHz and 10 K (black trace). Simulation using same parameters as in Table 1 ignoring the fourth order zfs parameter B_4^4 (blue trace) and including $B_4^4 = 18\times10^{-4}$ cm^{-1} (red trace). The dashed vertical lines mark the maxima of the respective simulated resonances; the field difference between them is ca. 6 mT. Isotropic single-crystal linewidth of 17 mT was used in the simulations. (For interpretation of the references to color in this figure legend, the reader is referred to the web version of this article.)

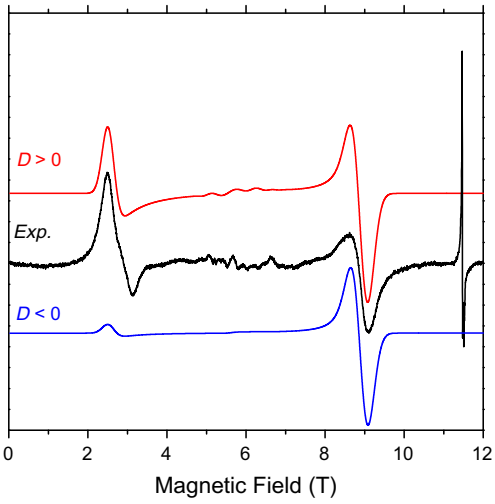

Fig. 4. HFEPR spectrum of $[Fe_{0.08}Zn_{0.92}(H_2O)_6]SiF_6$ at 321.6 GHz and 20 K. The black trace is experiment while the colored traced were simulated using: $|D| = 13.1$ cm^{-1}, $E = 0$, $g_\perp = 2.18$; $g_{||} = 2.00$. Red trace used a positive sign of D while blue trace – a negative sign of same parameter. Single-crystal linewidth: 200 mT (perpendicular) and 150 mT (parallel). The sharp peak near $g = 2.00$ (~11.5 T) belongs to impurities (including Mn(II) and presumably Fe(III)) and was not simulated. (For interpretation of the references to color in this figure legend, the reader is referred to the web version of this article.)

in analyzing the "X-band active signal" of a rhombic Mn(III) ($3d^4$) complex [47].

3.2. HFEPR spectroscopy of $[Fe_{0.08}Zn_{0.92}(H_2O)_6]SiF_6$

Since the hexaaquaferrous ion was also investigated in the literature in mixed systems where Fe(II) was doped into a diamagnetic host, we prepared and investigated a sample of $[Fe_{0.08}Zn_{0.92}(H_2O)_6]SiF_6$. This sample, measured as a powder, produced a similarly strong and well-defined HFEPR response relative to the pure (undoped) system. Fig. 4 shows a representative spectrum of $[Fe_{0.08}Zn_{0.92}(H_2O)_6]SiF_6$ at 321.6 GHz and 20 K accompanied by simulations, which substantiate the positive of sign of D even better than in the undoped system. Fig. S5 in the Supplementary Information shows a similar spectrum and simulations at 635 GHz and 20 K. Somewhat surprisingly, the linewidth of the observed resonances is increased rather than decreased in the magnetically diluted sample, which suggests that the spin–spin interactions between the Fe(II) ions are not the determining factor for that parameter. (The behavior of the impurities, on the other hand, shows the expected line narrowing upon magnetic dilution.)

The simulations suggested that the second-rank zfs parameters in the doped system are different from those in the pure complex. In order to determine them accurately, we followed our usual approach, and generated a 2-D map of resonances as a function of frequency (energy), shown in Fig. 5.

The striking feature of the 2-D map for $[Fe_{0.08}Zn_{0.92}(H_2O)_6]SiF_6$ is the presence of only one zero-field resonance at about 400 GHz, whereas in the pure $[Fe(H_2O)_6]SiF_6$ there are two; at ca. 300 and 415 GHz (Figs. 2 and 6). Since those two resonances in the latter case are separated by $6E$, this immediately suggests that the zfs tensor in $[Fe_{0.08}Zn_{0.92}(H_2O)_6]SiF_6$ is close to axial. However, E cannot be strictly zero, since Hendrich and Debrunner [1] reported an observation of the "X-band active transition" in $[Fe_{0.04}Zn_{0.96}(H_2O)_6]SiF_6$, which can occur only when $E \neq 0$. Indeed, even if we could not observe the corresponding splitting of the perpendicular turning points into x and y components, our best fits yielded an E value of 0.05 cm^{-1} in addition to $D = 13.42$ cm^{-1} (Table 2), which agrees well with the X-band value of 0.04 cm^{-1} [13].

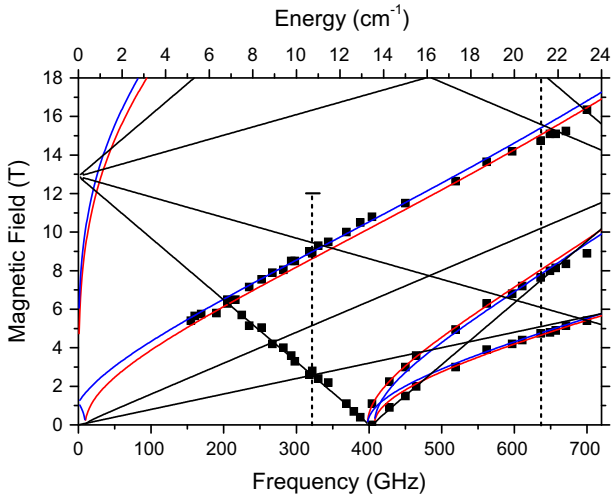

Fig. 5. A field/frequency map of resonances in $[Fe_{0.08}Zn_{0.92}(H_2O)_6]SiF_6$ at 10/20 K. Squares are experimental points while the curves were calculated using the best-fitted spin Hamiltonian parameters as in Table 2. Red traces: resonances with $B_0 \parallel x$, blue traces: with $B_0 \parallel y$, black traces: $B_0 \parallel z$. The vertical dashed line at 321.6 GHz represents the frequency and field range of the spectrum shown in Fig. 4 while that at 635 GHz represents the parameters of the spectrum shown in Fig. S5 in the Supplementary Information. (For interpretation of the references to color in this figure legend, the reader is referred to the web version of this article.)

3.3. FDMRS of $[Fe(H_2O)_6]SiF_6$ and $[Fe_{0.08}Zn_{0.92}(H_2O)_6]SiF_6$

To further investigate the rhombicity of the zfs tensor in $[Fe_{0.08}Zn_{0.92}(H_2O)_6]SiF_6$, we took a better look at the zero-field transition near 400 GHz by performing a zero-field FDMRS experiment in the 250–530 GHz frequency range. The resulting spectrum displays a doubling of the zero-field transition as shown in Fig. 6 (lower part). A best fit resulted in two Lorentzian-shaped absorption curves centered on 397.4 and 423.4 GHz, i.e., distanced from each other by 26 GHz. Assuming this value to represent $6|E|$, it translates into $E = 0.144\ cm^{-1}$. For comparison, we also show a FDMRS spectrum of the pure (undoped) sample of $[Fe(H_2O)_6]SiF_6$ and its simulation using two Lorentzian-shaped absorption curves centered on 295 and 418 GHz, respectively.

3.4. Comparison among experimental techniques

A comparison of spin Hamiltonian parameters extracted from multiple techniques for $[Fe(H_2O)_6]SiF_6$ highlights the remarkably high quality of the early HFEPR and FDMRS work on this system. The parameters obtained from our FDMRS spectra using BWOs as sub-THz sources ($D = 11.88$, $E = 0.68\ cm^{-1}$) are identical to those of Rubins and Fetterman [7], who used a Far-Infrared (FIR) Fourier Spectrometer and a BWO, and are virtually identical to those of Champion and Sievers [6], who employed exclusively FIR spectroscopy. The advantage of using solid-state sources and BWOs is the ease, and sensitivity, of experiments at sub-THz frequencies. On the other hand, the power emitted from both kinds of sources declines with increasing frequency, so that the sensitivity above 1 THz becomes problematic. In contrast, in FIR spectroscopy the sensitivity generally improves upon going to higher frequencies. This is why both FIR studies were also able to observe transitions from the excited $|S,M_S\rangle = |2,\pm1\rangle$ spin sublevels, which in $[Fe(H_2O)_6]SiF_6$ appear at 33.7 and 38 cm^{-1}.

Although both Champion and Sievers [6] and Rubins and Fetterman [7] reported HFEPR results on $[Fe(H_2O)_6]SiF_6$, the ease of performing this type of experiment has dramatically improved with the introduction of a new generation of sweepable superconducting magnets as illustrated by spectra shown in Figs. 1 and 4 as well as by use of EPR-quality resistive magnets illustrated by spectra shown in Figs. S1 and S5. When tunable-frequency sources (BWOs) are used in conjunction with a rapidly-swept (7 T/min) resistive magnet, it is possible to obtain within a reasonable time detailed 2-D maps of resonances in the field/frequency domain, such as those shown in Figs. 2 and 5. These maps enabled us to obtain second-order zfs parameters and g values to a high precision, with the additional advantage of obtaining the fourth-order zfs parameter B_4^0 for $[Fe(H_2O)_6]SiF_6$. Finally, adding the result of parallel-mode X-band EPR to the data set allowed us to determine the fourth-order zfs parameter B_4^4. It appears that the optimal methodology of obtaining accurate spin Hamiltonian parameters in a high-spin complex such as $[Fe(H_2O)_6]SiF_6$ is performing a zero-field FDMRS experiment to obtain seed zfs parameters followed by a multi-frequency high-field EPR experiment. The 2-D map of resonances obtained from the latter can be then fitted starting with the seed parameters obtained from former, and adding g-matrix elements. Eventually, all parameters can be varied to obtain an optimal fit. Also, parallel-mode X-band EPR is always useful for $S = 2$ systems as an independent control (and a widely available technique), and possibly to obtain additional fourth-order zfs parameters.

Magnetic resonance methods may not be always applicable to HS Fe(II) systems, particularly characterized by zfs parameters much larger than those of $[Fe(H_2O)_6]SiF_6$, or having negative D. In the first case, many transitions may not be observed within the 1 THz limit characterizing current sources. In the second case, resonances would be pushed up into yet higher fields than those easily generated with the current generation of magnets (see Fig. S1 for the case of negative D). It is therefore worth evaluating the quality of alternative techniques. Of those, magnetic measurements are always necessary on a previously uncharacterized

Table 2
Spin Hamiltonian parameters for $[Fe_xZn_{(1-x)}(H_2O)_6]SiF_6$.

D (cm^{-1})	$\lvert E\rvert$ (cm^{-1})	g_x	g_y	g_z	x	Ref., technique
+13.42(1)	0.05(1)	2.25(1)	2.22(1)	2.23(1)	0.08	This work, HFEPR [a]
13.68	0.144				0.08	This work, FDMRS
	0.04	2.26	2.26	2.40	0.04	X-band EPR [b]
+20.2		2.26	2.26	2.38	0.02	X- and K-band EPR [c]
14.3					0.15, 0.30	Magnetization [d]
15.3					0.15, 0.30	Mössbauer [d]
−0.12	0.0016	2.00	2.00	2.00	0.002	HFEPR [e]

[a] Fourth order terms (B_4^0, B_4^4) were not obtainable from the dataset for the doped complex due to lower S/N.
[b] Refs. [1,13].
[c] Ref. [4].
[d] Ref. [16].
[e] Ref. [27], averaged parameters from presumed two crystal sites. We have no good explanation as to why these results differ so much from the others in the table; the doping level may have been too low to be effective and the observed resonances could have originated from species other than HS Fe(II), for example from Mn(II), which is omnipresent in the starting materials.

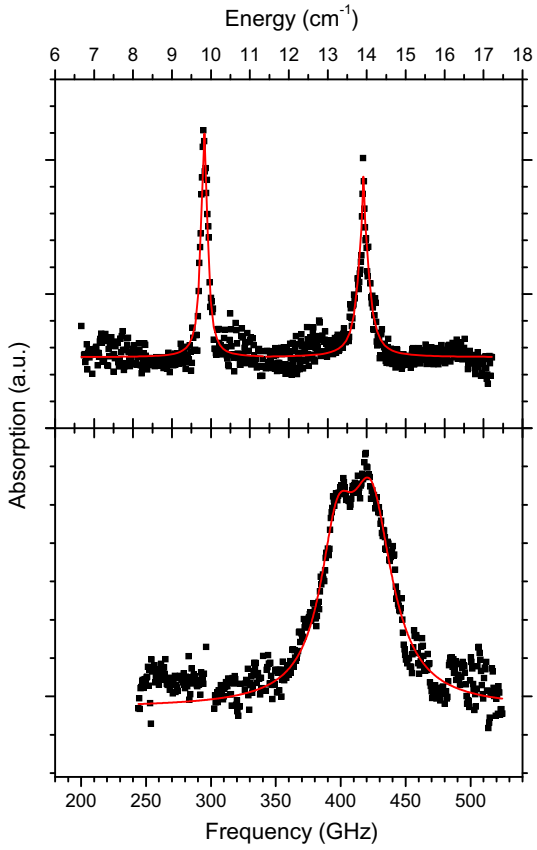

Fig. 6. FDMRS spectra of pure $[Fe(H_2O)_6]SiF_6$ at 1.5 K (top) and $[Fe_{0.08}Zn_{0.92}(H_2O)_6]SiF_6$ at 5 K (bottom). Squares are experimental points while the lines were drawn using two best-fitted Lorentzian curves in each case (center frequencies given in the text).

system, and if performed and analyzed properly, may deliver reasonably good data, although not as accurate and consistent as magnetic resonance. MCD appears to produce more dependable results, as discussed by Campochiaro et al. [19] and by some of us [48,49]. Quite interestingly, Raman scattering has also been able to detect the magnetic transitions in $[Fe(H_2O)_6]SiF_6$ [21] and deliver results that are virtually identical than those obtained by magnetic resonance, particularly in high field. The electronic Raman results are less precise than those from HFEPR, but have the advantage of a much higher energy range; Gnezdilov et al. observed electronic transitions at 47.6 cm^{-1} [21] involving the excited $|2,\pm2\rangle$ spin sublevels. We presume that in Raman, as with FIR spectroscopy, higher frequencies (i.e., further from the excitation band) are easier to observe.

3.5. The effect of crystal symmetry on the spectra

The most obvious difference in spin Hamiltonian parameters of the $[Fe(H_2O)_6]^{2+}$ ion in the pure crystal, and those in the doped $[Zn(H_2O)_6]SiF_6$ system is the rhombicity of the zfs tensor, amounting to about $|E/D| = 0.06$ in the pure compound. Although such a rhombicity appears in other hexaaqua ions of nominally high symmetry such as $[Mn(H_2O)_6]^{3+}$, where it was shown by Tregenna-Piggott et al. [50] as originating from the anisotropy of π-bonding between the metal ion and water molecules, the obvious and most intuitive reason for the rhombicity of the zfs tensor in $[Fe(H_2O)_6]SiF_6$ is the crystal symmetry lowering from axial at room temperature to rhombic (monoclinic) at low temperatures. This is best shown by the almost perfectly axial zfs tensor in the doped $[Fe_{0.08}Zn_{0.92}(H_2O)_6]SiF_6$ crystal, as $[Zn(H_2O)_6]SiF_6$ does not undergo symmetry lowering. The rhombicity in that case is not exactly zero (the rhombicity factor $|E/D| \sim 3 \times 10^{-3}$ was measurable by independent techniques) but is still very small and likely caused by the factors similar to those identified in $[Mn(H_2O)_6]^{3+}$.

Another striking feature of the doped $[Fe_{0.08}Zn_{0.92}(H_2O)_6]SiF_6$ complex is an increased linewidth of both zero-field, and high-field spectra compared to pure $[Fe(H_2O)_6]SiF_6$. This is counterintuitive, as magnetic dilution should in principle make the linewidth decrease rather than increase. At this point we do not have a ready explanation of this effect other than noting that evidently spin–spin interactions do not play a decisive role in determining the linewidth in this case. Speculatively, we may think of an inhomogeneous distribution of dopants in the host crystal as a possible reason for this phenomenon.

3.6. Optical spectra and ligand-field theory analysis of $[Fe(H_2O)_6]SiF_6$

Diffuse reflectance UV–Vis–NIR spectra of $[Fe(H_2O)_6]SiF_6$ qualitatively confirmed the original, higher resolution, multi-temperature optical studies by Agnetta et al. [20] and the more recent MCD work by Campochiaro et al. [19]. Comparison with spectra for the Zn analog showed no evidence for other than vibrational modes over the range 1400–2200 nm. $[Fe(H_2O)_6]SiF_6$ exhibits bands at 9600, 10,800, and 13,700 cm^{-1} [19,20]. The higher and lower of these have been assigned as transitions to (unspecified) triplet excited states and the middle one to the spin allowed $^5T_{2g} \rightarrow {}^5E_g$ (in O_h point group symmetry; $t_2^4e^2 \rightarrow t_2^3e^3$ in a strong field representation) transition. We felt that a more quantitative analysis could be made. The two spin-forbidden bands can be simultaneously fitted to within ~150 cm^{-1} (with the allowed band fitted exactly) using the following d^6 octahedral ligand-field parameters [51]: $B = 850(5)$ cm^{-1}, $C = 3650(25)$ cm^{-1}, $Dq = 1080$ cm^{-1}. These Racah parameters are each ~95% of their free-ion values [52,53], which is reasonable for a relatively non-covalent complex. This analysis shows that the band at 9600 cm^{-1} corresponds to $^5T_{2g} \rightarrow {}^3T_{1g}$ and that at 13,700 cm^{-1} corresponds to $^5T_{2g} \rightarrow {}^3T_{2g}$. Both triplet states correspond to $t_2^4e^2$ in a strong field representation (i.e., the same as the ground state) which may make them more allowed. The calculation indicates that the LS d^6 singlet state, $^1A_{1g}(t_2^6e^0)$ is at ~8800 cm^{-1}, and the next $^3T_{1,2g}$ states are at ~19,000–20,000 cm^{-1}. Our UV–Vis data suggest that there may be the onset of weak absorption at ~19,000 cm^{-1}, although the dominant feature is a charge transfer band extending into the UV region.

The complex is obviously not perfectly octahedral; however, we have no estimate for the magnitude of the trigonal distortion (i.e., a transition within the $^5T_{2g}$ ground state is not observable). There is, however, one important point to make which relates to the magnetic resonance studies. Trigonal distortion of the $^5T_{2g}$ ground state, whether from the Jahn–Teller effect, from π-bonding effects of the aqua ligands, from inter-ionic effects in the crystal, or any other source(s), splits this state into $^5A_{1(g)}$ and $^5E_{(g)}$ (in D_3 or D_{3d} symmetry; the g subscript is for the latter). If the ground state is ^5E, then it is highly unlikely that an $S = 2$ spin Hamiltonian would successfully describe the ground state electronic structure [54]. Unquenched orbital angular momentum in ^5E would give ten low lying states whose energies and spin behavior would not match those observed, which instead fit almost perfectly to an $S = 2$ spin Hamiltonian with zfs as described above. Use of the Ballhausen [51] parameter $Dt > 0$ gives a trigonal distortion with a $^5A_{1(g)}$ ground state and $^5E_{(g)}$ next excited state. In principle, it should be possible to include both trigonal splitting and spin–orbit coupling to reproduce the observed zfs. However, this is too unconstrained a parameter space. We therefore fixed the trigonal splitting somewhat arbitrarily and allowed B (with $C \equiv 4.3B$, as in the purely octahedral model), Dq, and ζ to vary. With

$Dt \equiv 150\ cm^{-1}$ [55], the fit yields (all values in cm^{-1}): $B = 814$, $C = 3500$, $Dq = 954$, and $\zeta = -400$, which gives $D = +13.2\ cm^{-1}$ (based on the first excited state doublet energy) in excellent agreement with experiment [56].

The calculation also finds ^5E centered at 10,875 cm^{-1}, in exact agreement with experiment, and the states originating in $^3T_{1g}$ in the range 9860–10,400 cm^{-1} (a barely significant discrepancy from experiment: ~50 nm in this poorly resolved NIR region) and those originating in $^3T_{2g}$ in the range 13,100–14,400 cm^{-1} (i.e., centered at exactly the observed band). While this is by no means a unique, or ideal, solution, it demonstrates that with reasonable input (the Racah and SOC parameters are all ~90% of the free-ion values) the optical and EPR characteristics of the $[Fe(H_2O)_6]^{2+}$ ion in the hexafluorosilicate salt can be successfully modeled by LFT.

3.7. Quantum chemical calculations

Having established highly precise and accurate values of the spin Hamiltonian parameters from HFEPR and FDMRS, and modeled them using a simple LFT approach, we then proceed to correlate these parameters with the available crystallographic data by quantum chemical calculations. This method directly addresses the structural distortion of the complex from ideal symmetry that was only approximated above. An attempt was thus undertaken to evaluate the g values and zfs parameters by both DFT and simple *ab initio* methods. The resulting zfs parameters from DFT (Table 3) are smaller than those obtained from experiment, as are the calculated deviations of g from g_e, indicating underestimation of spin–orbit coupling effects. The positive sign of D is reproduced, however. The failure of DFT to properly predict zfs in transition metal complexes and the superior performance of *ab initio* methods have been noticed previously [57].

UHF calculations were therefore performed followed by calculation of zfs through the 'coupled perturbed' treatment of the spin–orbit coupling contribution [58]. That method proved to be more successful than DFT, resulting in significantly larger calculated D values, while also giving more realistic g values. Consistent with LFT (Table 3), UHF gives one g value = 2.00 and two values >2.00, and the value $g = 2.00$ is oriented in the same direction as z (D_{zz}) and is thus g_z ($g_{||}$).

Indeed, the parameter match for the doped complex is excellent (see Table 3), which is significant since in this case the structure of the material examined by HFEPR is that determined crystallographically. The discrepancies for the pure complex may well be due to the difference in structure, although we have no way of proving this except to note that the relatively larger E value is corroborated by the proposed lower symmetry of the low temperature phase [23,29,31]. As pointed out by Carver et al. in their study of $[CsFe(H_2O)_6]PO_4$ [59], very small structural distortions can have a strong effect on the zfs. We believe that more sophisticated *ab initio* methods, such as CASSCF and SORCI [57] should be applied to $[Fe(H_2O)_6]^{2+}$, but such efforts are beyond the scope of this primarily spectroscopic study.

Table 3
Comparison of the results of theory calculations to the experimental spin Hamiltonian parameters.

Complex/method	D (cm^{-1})	$\|E\|$ (cm^{-1})	g_x	g_y	g_z
$FeSiF_6{\cdot}6H_2O$[a]					
Experiment	+11.97	0.65	2.08	2.13	2.00
DFT	+3.54	0[c]	2.04	2.04	2.00
UHF	+7.77	0[c]	2.12[d]	2.12[d]	2.00[d]
$Fe_{0.08}Zn_{0.92}SiF_6{\cdot}6H_2O$[b]					
Experiment	+13.42	0.05	2.25	2.22	2.23
DFT	+4.43	0.02	2.05	2.05	2.00
UHF	+12.33	0.02	2.22[d]	2.22[d]	2.002[d]
LFT [e]	+13.2	0	2.29	2.29	2.00

[a] Using $[Fe(H_2O)_6]SiF_6$ high-temperature phase structure [29].
[b] Using $[Zn(H_2O)_6]SiF_6$ structure [32].
[c] We used the high-temperature, high-symmetry phase for calculations, details of the low-temperature phase remaining unknown. This explains the calculated axial zfs tensor.
[d] The ORCA output assigns the g value = 2.00(2) as g_x, but also associates it with the principal (parallel) direction of zfs (D_{zz}) and thus the correct assignment is actually as g_z ($g_{||}$); the g values = 2.12 (2.22) are associated with the perpendicular zfs direction and are thus g_x ($g_\perp$).
[e] Ligand-field theory calculation using the d^6 basis set with (all values in cm^{-1}): $B = 814$, $C = 3500$, $Dq = 954$, $Dt = +150$, $\zeta = -400$ (negative for d^6), which necessarily gives an axial zfs. The isotropic orbital reduction parameter, $k = 0.9$, was also used so as to correspond to the ~90% reduction from the free-ion values for the Racah and SOC parameters. Addition of a magnetic field (0–10 T) along each of the x (same as y) and z directions allowed calculation of g values as described in the Supplementary Material. These results directly associate $g = 2.00$ as g_z.

4. Conclusions

The high spin hexaaquaferrous ion in the form of the pure complex $[Fe(H_2O)_6]SiF_6$ and the doped complex $[Fe_{0.08}Zn_{0.92}(H_2O)_6]SiF_6$ can be readily examined by HFEPR and FDMRS to give high quality, easily interpreted spectra, which in turn give precise and accurate information on the spin Hamiltonian parameters of this ion, including fourth order zfs terms for the pure complex. These results are corroborated by pioneering studies using these and other techniques such as electronic Raman spectroscopy. Slight structural differences between the pure complex and the Zn host are reflected in the spin Hamiltonian parameters. Both classical LFT and modern quantum chemistry computations can be applied to this complex as a paradigm for HS Fe(II). LFT suggests that the ground state is $^5A_1$, which allows the successful application of the spin Hamiltonian model. We speculate that it is this orbitally nondegenerate ground state that has contributed to making $[Fe(H_2O)_6]SiF_6$ more amenable to study by magnetic resonance techniques than other HS ferrous salts. LFT was also able to reproduce the optical and EPR parameters of the complex although the parameter set, while quite reasonable, cannot be considered as the definitive solution. DFT is only moderately successful at reproducing the parameters; however, UHF is quite successful in this effort. We hope that the methods used in this study will inspire similar experimental work on HS Fe(II) in other systems, especially those in bioinorganic chemistry.

Acknowledgments

This work has been supported by the NHMFL, which is funded by NSF (Cooperative Agreement DMR 0654118), the State of Florida, and DOE. JK and JT received additional funds from User Collaboration Grant 5062. The 25-T resistive magnet was funded by the W. Keck Foundation. The UV-Vis-NIR spectrophotometer at Roosevelt U. was obtained thanks to the Goldenberg Foundation. CS was paid by IMPRS-AM.

Appendix A. Supplementary data

Supplementary data associated with this article can be found, in the online version, at doi:10.1016/j.jmr.2011.09.046.

References

[1] M.P. Hendrich, P.G. Debrunner, EPR spectra of quintet ferrous myoglobin and a model heme compound, J. Magn. Reson. 78 (1988) 133–141.
[2] M.P. Hendrich, P.G. Debrunner, Integer-spin electron paramagnetic resonance of iron proteins, Biophys. J. 56 (1989) 489–506.
[3] R. Song, P.E. Doan, R.J. Gurbiel, B.E. Sturgeon, B.M. Hoffman, Non-Kramers ENDOR and ESEEM of the $S = 2$ ferrous ion of $[Fe(II)EDTA]^{2-}$, J. Magn. Reson. 141 (1999) 291–300.

[4] R.S. Rubins, On the paramagnetic resonance spectrum of divalent iron in zinc fluosilicate, Proc. Phys. Soc. 80 (1962) 244–247.
[5] J.T. Vallin, G.A. Slack, C.C. Bradley, Far-infrared absorption of ZnS:Fe^{2+} in strong magnetic fields, Phys. Rev. B 2 (1970) 4406–4413.
[6] P.M. Champion, A.J. Sievers, Far infrared magnetic resonance in $FeSiF_6{\cdot}6H_2O$ and $Fe(SPh)_4^{2-}$, J. Chem. Phys. 66 (1977) 1819–1825.
[7] R.S. Rubins, H.R. Fetterman, Electron paramagnetic resonance in ferrous fluosilicate at submillimeter wavelengths, J. Chem. Phys. 71 (1979) 5163–5166.
[8] M.J. Knapp, J. Krzystek, L.-C. Brunel, D.N. Hendrickson, High-frequency EPR study of the ferrous ion in the reduced rubredoxin model $[Fe(SPh)_4]^{2-}$, Inorg. Chem. 39 (2000) 281–288.
[9] G. Carver, P.L.W. Tregenna-Piggott, A.-L. Barra, A. Neels, J.A. Stride, Spectroscopic and structural characterization of the $[Fe(imidazole)_6]^{2+}$ cation, Inorg. Chem. 42 (2003) 5771–5777.
[10] A. Ozarowski, S.A. Zvyagin, W.M. Reiff, J. Telser, L.-C. Brunel, J. Krzystek, High-frequency and -field EPR of a pseudo-octahedral complex of high-spin Fe(II): bis(2,2′-bi-2-thiazoline)bis(isothiocyanato)iron(II), J. Am. Chem. Soc. 126 (2004) 6574–6575.
[11] J. Telser, J. van Slageren, S. Vongtragool, M. Dressel, W.M. Reiff, S.A. Zvyagin, A. Ozarowski, J. Krzystek, High-frequency and -field EPR spectroscopy of the high-spin ferrous ion in hexaaqua complexes, Magn. Reson. Chem. 43 (2005) S130–S139.
[12] A.L. Barra, A.K. Hassan, A. Janoschka, C.L. Schmidt, V. Schunemann, Broad-band quasi-optical HF-EPR spectroscopy: application to the study of the ferrous iron center from a rubredoxin mutant, Appl. Magn. Reson. 30 (2006) 385–397.
[13] R.S. Rubins, T.D. Black, Electron paramagnetic resonance in ferrous fluosilicate near 10 K, Chem. Phys. Lett. 81 (1981) 450–452.
[14] L.C. Jackson, The magnetic susceptibility of ferrous fluosilicate at low temperatures, Philos. Mag. Ser. 8 (4) (1959) 269–272.
[15] T. Ohtsuka, Crystalline field splitting in ferrous fluosilicate, J. Phys. Soc. Jpn. 14 (1959) 1245–1245.
[16] F. Varret, Pulsed magnetic field study of Fe^{2+} in some fluosilicates, J. Phys. Chem. Solids 37 (1976) 257–263.
[17] F. Varret, Y. Allain, A. Meidan-Gros, Direct investigation of spin hamiltonians DS_z^2 by measuring magnetization during intense pulsed fields, Solid State Commun. 14 (1974) 17–20.
[18] F. Varret, F. Hartmann-Boutron, Effets du couplage spin-orbite sure les proprietés des composés magnetiques ioniques du groupe du fer a températures de transition basse, Ann. Phys. 3 (1968) 157–168.
[19] C. Campochiaro, E.G. Pavel, E.I. Solomon, Saturation magnetization magnetic circular dichroism spectroscopy of systems with positive zero-field splittings: application to $FeSiF_6{\cdot}6H_2O$, Inorg. Chem. 34 (1995) 4669–4675.
[20] G. Agnetta, T. Garofano, M.B. Palma-Vittorelli, M.U. Palma, Low-temperature optical absorption of ferrous fluosilicate crystals, Philos. Mag. 7 (1962) 495–498.
[21] V.P. Gnezdilov, V.V. Eremenko, A.V. Peschansky, V.I. Fomin, The Raman scattering by low-energy electronic excitation of Fe^{2+} in ferrous fluosilicate (in Russian), Fiz. Niz. Temp. 17 (1991) 253–258.
[22] C.E. Johnson, Hyperfine interactions in ferrous fluosilicate, Proc. Phys. Soc. 92 (1967) 748–757.
[23] H. Spiering, R. Zimmermann, G. Ritter, Investigation of hyperfine interaction and structure in $FeSiF_6{\cdot}6H_2O$ by Mössbauer measurements, Phys. Stat. Sol. (b) 62 (1974) 123–133.
[24] C. Rudowicz, Theoretical spin Hamiltonians for 3 d^n ions with $S = 2$ compared to direct investigation by the method of Varret et al., Solid State Commun. 15 (1974) 1937–1940.
[25] Y.-Y. Zhou, M.-G. Zhao, Theoretical study of phase transformation in ferrous fluosilicate using EPR and optical spectra, J. Phys. C: Solid State Phys. 20 (1987) 5097–5103.
[26] Z. Li, X.-Y. Kuang, T.-F. Yang, Y. Li, Theoretical study of spin-singlet contributions to zero-field splitting of a $3d^6$ ion in a trigonal ligand field and applications to Fe^{2+} in $FeSiF_6{\cdot}6H_2O$ and $FeCO_3$, Mol. Phys. 106 (2008) 2677–2683.
[27] S.K. Misra, S. Diehl, D. Tipikin, J.H. Freed, A multifrequency EPR study of Fe^{2+} and Mn^{2+} ions in a $ZnSiF_6{\cdot}6H_2O$ single crystal at liquid-helium temperatures, J. Magn. Reson. 205 (2010) 14–22.
[28] R.W.G. Wyckoff, Crystal Struct. 3 (1951) 797.
[29] W.C. Hamilton, Bond distances and thermal motion in ferrous fluosilicate hexahydrate: a neutron diffraction study, Acta Crystallogr. 15 (1962) 353–360.
[30] G. Chevrier, A. Hardy, G. Jéhanno, Antiphase périodique orientationnelle et transformation de phase dans le fluosilicate de fer, Acta Crystallogr. A 37 (1981) 578–584.
[31] G. Jehanno, F. Varret, Structural disorder and phase transformationin fluosilicated of Fe, Mg, and Mn, Acta Crystallogr. A 31 (1975) 857–858.
[32] S. Ray, A. Zalkin, D.H. Templeton, Crystal structures of the fluosilicate hexahydrates of cobalt, nickel and zinc, Acta Crystallogr. B 29 (1973) 2741–2747.
[33] S.A. Zvyagin, J. Krzystek, P.H.M. van Loosdrecht, G. Dhalenne, A. Revcolevschi, Field-induced structural evolution in the spin-Peierls compound CuGeO3: high-field ESR study, Phys. Rev. B 67 (2003) 212403.
[34] A.K. Hassan, L.A. Pardi, J. Krzystek, A. Sienkiewicz, P. Goy, M. Rohrer, L.-C. Brunel, Ultrawide band multifrequency high-field EMR technique: a methodology for increasing spectroscopic information, J. Magn. Reson. 142 (2000) 300–312.
[35] J. van Slageren, S. Vongtragool, B. Gorshunov, A.A. Mukhin, N. Karl, J. Krzystek, J. Telser, A. Müller, C. Sangregorio, D. Gatteschi, M. Dressel, Frequency-domain magnetic resonance spectroscopy of molecular magnetic materials, Phys. Chem. Chem. Phys. 5 (2003) 3837–3843.
[36] A. Abragam, B. Bleaney, Electron Paramagnetic Resonance of Transition Ions, Dover Publications, Inc., New York, 1986.
[37] J. Krzystek, S.A. Zvyagin, A. Ozarowski, S. Trofimenko, J. Telser, Tunable-frequency high-field electron paramagnetic resonance, J. Magn. Reson. 178 (2006) 174–183.
[38] F. Neese, ORCA – An *ab initio*, Density Functional and Semiempirical Program Package, Universität Bonn, Bonn, Germany, 2010.
[39] The Ahlrichs auxiliary basis sets were obtained from the TurboMole basis set library at ftp.chemie.uni-karlsruhe.de/pub/jbasen.
[40] A. Schäfer, H. Horn, R. Ahlrichs, Fully optimized contracted Gaussian basis sets for atoms Li to Kr, J. Chem. Phys. 97 (1992) 2571–2577.
[41] D.A. Becke, Density-functional exchange-energy approximation with correct asymptotic behavior, Phys. Rev. A 38 (1988) 3098–3100.
[42] K. Eichkorn, O. Treutler, H. Öhm, M. Häser, R. Ahlrichs, Auxiliary basis sets to approximate Coulomb potentials, Chem. Phys. Lett. 240 (1995) 283–289.
[43] K. Eichkorn, O. Treutler, H. Öhm, M. Häser, R. Ahlrichs, Erratum to Auxiliary basis sets to approximate Coulomb potentials (Chem. Phys. Lett. 240 (1995) 283), Chem. Phys. Lett. 242 (1995) 652–660.
[44] K. Eichkorn, F. Weigend, O. Treutler, R. Ahlrichs, Auxiliary basis sets for main row atoms and transition metals and their use to approximate Coulomb potentials, Theor. Chem. Acc. 97 (1997) 119–124.
[45] F. Weigend, R. Ahlrichs, Balanced basis sets of split valence, triple zeta valence and quadruple zeta valence quality for H to Rn: design and assessment of accuracy, Phys. Chem. Chem. Phys. 7 (2005) 3297.
[46] G. Aromí, J. Telser, A. Ozarowski, L.-C. Brunel, J. Krzystek, Synthesis, crystal structure, and high precision high-frequency and -field electron paramagnetic resonance investigation of a Mn(III) complex: $[Mn(dbm)_2(py)_2](ClO_4)$, Inorg. Chem. 44 (2005) 187–196.
[47] J. Krzystek, G. Yeagle, J.-H. Park, M.W. Meisel, R.D. Britt, L.-C. Brunel, J. Telser, High frequency and field EPR spectroscopy of tris(2,4-pentanedionato)manganese(III): investigation of solid-state versus solution Jahn–Teller effects, Inorg. Chem. 42 (2003) 4610–4618.
[48] J. Krzystek, A.T. Fiedler, J.J. Sokol, A. Ozarowski, S.A. Zvyagin, T.C. Brunold, J.R. Long, L.-C. Brunel, J. Telser, Pseudo-octahedral complexes of vanadium(III): electronic structure investigation by magnetic and electronic spectroscopy, Inorg. Chem. 43 (2004) 5645–5658.
[49] J. Krzystek, S.A. Zvyagin, A. Ozarowski, A.T. Fiedler, T.C. Brunold, J. Telser, Definitive spectroscopic determination of zero-field splitting in high-spin cobalt(II), J. Am. Chem. Soc. 126 (2004) 2148–2155.
[50] P.L.W. Tregenna-Piggott, H. Weihe, A.-L. Barra, High-field, multifrequency EPR study of the $[Mn(OH_2)_6]^{3+}$ cation: influence of π-bonding on the ground state zero-field-splitting parameters, Inorg. Chem. 42 (2003) 8504–8508.
[51] C.J. Ballhausen, Introduction to Ligand Field Theory, McGraw-Hill, New York, 1962.
[52] J. Bendix, M. Brorson, C.E. Schäffer, Accurate empirical spin orbit coupling parameters ζ_{nd} for gaseous nd_q transition metal ions. The parametrical multiplet term model, Inorg. Chem. 32 (1993) 2838–2849.
[53] M. Brorson, C.E. Schäffer, Orthonormal interelectronic repulsion operators in the parametrical d^q model. Application of the model to gaseous ions, Inorg. Chem. 27 (1988) 2522–2530.
[54] B.R. McGarvey, J. Telser, Inorg. Chem., submitted for publication.
[55] This gives a trigonal splitting within $^5T_{2g}$ of $\sim$1000 cm^{-1} in the absence of SOC.
[56] The zfs of the doped Zn complex was fitted since this case is nearly axial. The higher spin doublet is at 55.0 cm^{-1} above the ground singlet, as opposed to the value of 52.8 cm^{-1} (4D) which would be expected for an $S = 2$ spin Hamiltonian without higher order terms, which further justifies the use of these terms in analyzing the HFEPR data. If only the ^5D basis set is used, rather than the complete d^6 basis set, with the same parameters ($\lambda = -100$ cm^{-1}) then the first excited state spin doublet is at 10.8 cm^{-1} above the ground singlet and the second excited spin doublet is at 46.2 cm^{-1} (not 43.2 = 4D), demonstrating both the contribution of triplet excited states to the zfs and the need for higher order spin Hamiltonian terms.
[57] S. Ye, F. Neese, A. Ozarowski, D. Smirnov, J. Krzystek, J. Telser, J.-H. Liao, C.-H. Hung, W.-C. Chu, Y.-F. Tsai, R.-C. Wang, K.-Y. Chen, H.-F. Hsu, Family of V(III)-tristhiolato complexes relevant to functional models of vanadium nitrogenase: synthesis and electronic structure investigations by means of high-frequency and -field electron paramagnetic resonance coupled to quantum chemical computations, Inorg. Chem. 49 (2010) 977–988.
[58] F. Neese, Calculation of the zero-field splitting tensor on the basis of hybrid density functional and Hartree–Fock theory, J. Chem. Phys. 127 (2007) 164112.
[59] G. Carver, C. Dobe, T.B. Jensen, P.L.W. Tregenna-Piggott, S. Janssen, E. Bill, G.J. McIntyre, A.-L. Barra, Spectroscopic, magnetochemical, and crystallographic study of cesium iron phosphate hexahydrate: Characterization of the electronic structure of the iron(II) hexa-aqua cation in a quasicubic environment, Inorg. Chem. 45 (2006) 4695–4705.